Influence of Control Strategy in Risk Mitigation of Building Damage Due to Earthquake

Normaisharah Mamat (normysarahmn@gmail.com)
Universiti Teknologi Malaysia https://orcid.org/0000-0002-6502-5327
Mohd Fauzi othman
Universiti Teknologi Malaysia
Mohd Fitri Mohd Yakub
Universiti Teknologi Malaysia

Research Article

Keywords: Control strategy, Deep learning, Collapse probability, Building damage, Enhance building safety

Posted Date: January 19th, 2022

DOI: https://doi.org/10.21203/rs.3.rs-892300/v2

INFLUENCE OF CONTROL STRATEGY IN RISK MITIGATION OF BUILDING DAMAGE DUE TO EARTHQUAKE

Normaisharah Mamat[1], Mohd Fauzi Othman[2], Fitri Yakub[3]

[1,2,3]Department of Electronic System Engineering,
Malaysia-Japan International Institute of Technology, Universiti Teknologi Malaysia,
Jalan Sultan Yahya Petra, 54100 Kuala Lumpur, Malaysia
Email: normaisharah@utm.my

Abstract

Building structures are prone to damage due to natural disasters, and this challenges structural engineers to design safer and more robust building structures. This study is conducted to prevent these consequences by implementing a control strategy that can enhance a building's stability and reduce the risk of damage. Therefore, to realize the structural integrity of a building, a hybrid control device is equipped with control strategies to enhance robustness. The control strategy proposed in this study is adaptive nonsingular terminal sliding mode control (ANTSMC). ANTSMC is an integrated controller of radial basis function neural network (RBFNN) and nonsingular terminal sliding mode control (NTSMC), which has a fast dynamic response, finite-time convergence, and the ability to enhance the control performance against a considerable uncertainty. The proposed controller is designed based on the sliding surface and the control law. The building with a two-degree-of-freedom (DOF) system is designed in Matlab/Simulink and validated with the experimental work connected to the LMSTest.Lab software. The performance of this controller is compared with those of the terminal sliding mode control (TSMC) and NTSMC in terms of the displacement response, sliding surface, and the probability of damage. The result showed that the proposed controller, ANTSMC can suppress vibrations up to 46%, and its percentage probability of complete damage is 15% from the uncontrolled structure. Thus, these findings are imperative towards increasing the safety level in building structures and occupants, and reducing damage costs in the event of a disaster.

Keywords

Control strategy. Deep learning. Collapse probability. Building damage. Enhance building safety

1. Introduction

Alleviating the structural building response in the event of an earthquake becomes an increasingly challenging task. The forces of nature threaten human existence, cause financial losses and environmental destruction. Large magnitude earthquakes damage properties and structures, and cause casualties. The earthquake magnitude of greater than 5.0 Mw may cause slight damage to the structures and buildings. The earthquake magnitude of greater than 6.0 Mw causes a lot of damage in a populated area. Moreover, major earthquakes that wreak severe damage occur at 7.0 Mw or higher. The higher moment magnitude with 8.0 Mw above will cause totally destroy to the community near the seismic location (Abu-Faraj et al. 2008; Grünthal and Musson 2020). A tool known as HAZUS is used to estimate the existing building stock potential of losses caused by earthquake ground motion. HAZUS estimates the economic, physical, and social impacts of a disaster by using the geographic information system through an agency called the Federal Emergency Management Agency (FEMA). The estimation of the losses estimation is crucial for preparedness plans and rehabilitation strategies of building stocks from earthquake disasters (Duan and Pappin 2008). Besides, the HAZUS damage functions is used to simulate the vulnerability of various types of structural buildings and it provides the information on deriving the building fragility curves for various types of structures consist of the probability of slight, moderate, extensive, and complete structural damage states (Vazurkar and Chaudhari 2016; Peyghaleh et al. 2018).

Robinson et al. (2018) shows empirically derived structural fragility curves of different building types. According to the fragility curves, at 0.4 g, the building made from stone and mud has 98% probability of collapsing. The earthquake effect causes many fatalities based on the 2015 Gorkha earthquake with the recorded magnitude of 7.3 Mw to 8.8 Mw. The curves show that at the magnitude of 8.6 Mw, the number of fatalities was up to 100,000, and at the magnitude of 7.3 Mw, the earthquake caused more than 50,000 fatalities.

Giordano et al. (2021) examined the fragility of the structural building made of masonry, RC frame, steel frame and timber frame. This vulnerability assessment study can be adopted to assess the possible loss of Nepal's school infrastructure due to an earthquake. The structural damage fragility curves can be categorized into several damage states, namely slight, moderate, extensive, and complete damage. In slight damage, small plaster cracks are formed at window and door corners. In the moderate state, larger cracks are formed at the window and door corners across the shear wall panel. Meanwhile, in the extensive damage condition, large diagonal cracks across the shear wall panel and permanent lateral movement of floors and roof are formed. Lastly, the complete damage state condition is detected by a large permanent lateral displacement or imminent danger of collapse (Federal Emergency Management Agency (FEMA) 2003; Alam et al. 2017).

Ansal et al. (2010) illustrated the cumulative damage probability curve for low-rise, mid-rise and high-rise reinforce concrete frame building. Other than the material of the building, the high of the building influence the probability of building damage. Martins and Silva (Martins and Silva 2020) have developed an analysis on the fragility and vulnerability of the most common building classes cover with the combination of structure material, height, lateral load resisting system and seismic design level. Incremental dynamic analysis (IDA) is a powerful tool of seismic engineering that performed to derived fragility curves for the various structures. It was developed based on the result of a probabilistic seismic hazard analysis to estimate the seismic risk faced by a particular structure (Vamvatsikos and Cornell 2002; Gkimprixis et al. 2020). Bayrak et al. (2021) reported that earthquake had caused severe damage, partial or total collapse of many buildings. Consequently, the fatalities, livestock industry and heritage buildings are affected (D'Ayala and Ansal, 2012). An earthquake warning system that delivers the ground shaking alert known as earthquake early warning (EEW) can be used as a precautionary tool to provide the society to take action before an incoming earthquake occurs. However, this tool has an obstacle in delivering false and missed EEW alarms especially for mid and high-rise buildings due to these buildings shaking occurrence may be different from the shaking at the ground (Allen and Melgar 2019; Cremen et al. 2021). Moreover, Gupta et al. (2020) mention that it is difficult to predict when and where the earthquake will occur. Even if an earthquake can be predicted, the society is not safe as well.

Therefore, innovative seismic solutions must be produced to overcome structural failures and defects. Hence, structural control for buildings is needed to provide safety and more efficient designs to prevent the structures from destruction. Moreover, structural vibration control has attracted more attention due to its robustness in eliminating vibrations. The technique can be categories into passive, active control, semi-active and hybrid control device (Xu 2014; Bhaiya et al. 2019; Zizouni et al. 2019). Among the structural control device, hybrid mass damper (HMD) has a prominent character that combines an active mass damper and a tuned mass damper (TMD) in a control device and it is found to be cost-effective by reducing energy requirement in their operation (Thenozhi and Yu 2013). Mitchell et al. (2013) investigated the performance of structures by implementing HMD and other control devices. The structure has used a variety of input excitations to observe the effectiveness of the control device in reducing the structural response. It was found that the implementation of HMD produced better control performance than the passive device for most cases. Then in 2017, Djedoui et al. (2017) investigated the hybrid control consisting of base isolator, TMD and HMD to their structure system. Base isolators which are installed between the foundation and the superstructure are some of the most widely used devices for vibration control. However, the floor acceleration and the inter-story drift are increased, resulting in an adverse effect on the structure. The efficiency of the base isolator depends on the type of excitation. A control signal required to suppress the building vibration is produced using a control algorithm measured by the structural response. Based on the control signal, the actuator will generate the secondary vibration response, decreasing the overall building vibration. Zamani et al. (2018) proposed adaptive fractional order fuzzy proportional-integral-derivative control strategy at smart base-isolate structure to control seismic. The fuzzy rule weight was adaptively tuned based on the values of the velocity of ground floor and the acceleration of the top floor. The proposed control strategy had a better response in decreasing the maximum base displacement and structure acceleration of the earthquake excitation given.

Chesne and Colette (2018) performed experimental validation of fail-safe HMD using a single DOF structure. They introduced a compensator into the feedback loop by actively softening the actuator to increase the stability margins of the control system. Then the same author proposed HMD to the structure system in 2017 by introducing a new control law for hybrid vibration absorbers referred to as α-HMD. α-HMD requires smaller active forces and less energy for the active element than the AMD and TMD (Chesné et al. 2019). In recent years, some researchers were interested in the theory of finite time mechanisms. Therefore, TSMC with this characteristic is introduced to overcome the problem caused by sliding mode control which involves in finite time state convergence. As a result, TSMC attracts widespread attention and is known as a nonlinear switching manifold, whereas the state will reach equilibrium in a finite time (Cao et al. 2013). The derivation of TSMC can be found in the study proposed by Liu

and Wang (2012). According to Cao et al. (2013), TSMC causes singularity to occur if the initial conditions are not appropriately selected will cause an infinite control law.

Nonsingular terminal sliding mode control (NTSMC) has an advantage in giving a fast dynamic response, finite-time convergence, high control precision and eliminating the paranormal phenomenon in the control input of the system (Xu et al. 2015). NTSMC has been applied in spacecraft, vehicles and rigid manipulators to eliminate singularity problems associated with TSMC (Zhu and Yan 2014; Ning et al. 2018). In 2019, Ba et al. (2019) modified NTSMC with an adaptive time-delay estimation technique. This controller is used to track the position of servomotor-actuated robotic systems. Lastly, the proposed controller successfully verifies the servomotor robot in a real-time 2-DOF different working conditions. The collaboration of the deep learning method with NTSMC enhances the robustness of the system control, which is RBFNN that has good generalization, simple network structure, fast learning, and can improve the control performance against considerable uncertainty of the system (Liu 2013). Deep learning is a subset of machine learning methods based on artificial neural networks. In cases of earthquakes, as Xing et al. (2020) investigated, machine learning able to predict the casualties of an earthquake disaster. The technique proposed by the authors provided accurate prediction and efficient learning, making it suitable for large sample sampling and small sample data fitting. Due to the advantages of RBFNN, this technique is chosen to collaborate with NTSMC. The function of RBFNN in TSMC is to predict the upper bound of an uncertain parameter. The detailed study and the derivation of RBFNN method can be found in the studies by combined RBFNN with TSMC to control robot manipulators. This controller is used to estimate all the system parameters via Gee-Lee matrix and its produce operators. The application of ANTSMC in robot manipulators shows that the proposed controller effectively controls the nonlinear system with robustness even under model changes and parameter uncertainties.

The majority of the previous studies applied this controller in the vehicle, robotic and spacecraft systems. However, no empirical evidence on the influence of a control strategy in minimizing the risk of building damage has been found to date. This control strategy, on the other hand, has excellent vibration control characteristics. As the improvement from (Mamat et al. 2020), this paper highlights the proposed control strategy, ANTSMC impact in mitigate the structural building from having damage that compare to NTSMC and TSMC . Each proposed control strategies demonstrate their efficiency in reducing the probability of the building to have damage and collapse by minimize the vibration during earthquake occur. ANTSMC integrates the deep learning technique to estimate the desired value in NTSMC. The deep learning technique has the ability to find appropriate value to fit the unknown value in the control strategy used. All the proposed control strategies demonstrate well response regarding their influence in mitigate the vibration. Moreover, the building structure representing mass, spring and damper is constructed in Simulink and validated via an experimental setup connected to LMS Test.Lab software. Many shaking table test has been tested by others researcher and just a few of them using shaking table test that connected to this software. Therefore, this study presented the details on experimental work that assembled and connected to LMS Test.Lab sofware. The result from the experimental work has strengthened the building structure that has been built in simulation.

2. System Design

2.1 Building structure

The building structure is represented by the mass, spring and damper system that consists of two DOFs. The controlling device, HMD is installed at the top floor of the building. The building structure and its free body diagram for the system is shown in Figure 1 and Figure 2, respectively. The mathematical model for the building structure are shown as (1), (2) and (3) where m_1 and m_2 denote the mass for each storey. $k_1$and k_2 denote the stiffness value and while c_1 and c_2 are damping coefficients for each storey. m_d, c_d and k_d are mass, damping and stiffness for HMD. The displacement responses for each floor and the control device are defined as x_1, x_2 and x_d. $\ddot{x}_g$ is the acceleration of the ground motion.

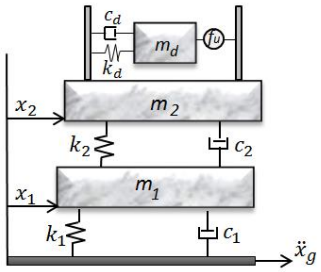

Figure 1 Building structure system for the 2-DOF system

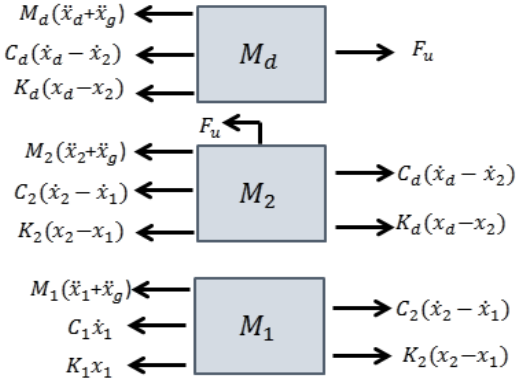

Figure 2 Free body diagram for the 2-DOF structure

$$M_1\ddot{x}_1 + C_1\dot{x}_1 + K_1x_1 - C_2(\dot{x}_2 - \dot{x}_1) - K_2(x_2 - x_1) = -M_1\ddot{x}_g \quad (1)$$

$$M_2\ddot{x}_2 + C_2(\dot{x}_2 - \dot{x}_1) + K_2(x_2 - x_1) - C_d(\dot{x}_d - \dot{x}_2) - K_d(x_d - x_2) = -M_2\ddot{x}_g - F_u \quad (2)$$

$$M_d\ddot{x}_d + C_d\dot{x}_d + K_dx_d - C_d\dot{x}_2 - K_dx_2 = -M_d\ddot{x}_g + F_u \quad (3)$$

An actuator is implemented to control HMD, and it is written as;

$$Ri + K_e(\dot{x}_d - \dot{x}_2) = F_u \quad (4)$$

$$F_u = K_f i \quad (5)$$

where K_f is the thrust constant, K_e is the induced voltage constant, R is the resistance value, F_u is the control force generated by the actuator, and i is current.

2.2 Experimental work

The experimental work is assembled as shown in Figure 3, the assembly is consist of the shaker, amplifier, mobile Signal Conditioning and Data Acquisition System (SCADAS), accelerometer and the miniature of 2-DOF building structure. Electrodynamic exciter (S 50350/LS-120), known as shaker, generates vibrations that can be operated either in a horizontal or vertical position. In this case, the vibration of the shaker is set up to a vertical position to reproduce similar seismic movement. The power amplifier received the signal from the input and frontend into the shaker. The voltage or current required by the amplifier depends on the size of the tested system and levels of the target vibration. The accelerometer is used to measure the movement of basement and mass at each floor. The sensitivity of the accelerometer is choosen based on the maximum vibration level. SCADAS is a modular data acquisition device which consists of the frame for housing components containing all the cards, controller and power supply. The power supply includes the battery for autonomous operation, where for this model the duration of battery

is around 2.5 hours. The mobile controller card is an ethernet interface linked with the Test.Lab software installed in the personal computer (PC) which consists of two output sources and two encoder inputs. SCADAS is used to capture dynamic signals, measure the accelerometer data and link the PC with Test.Lab software with amplifier. The LMS Test.Lab software was used to control the shaker and received the data from the experimental work. This software is designed as the solution for testing the equipment involved with vibration testing. It also offers quick visualization, easy reporting, and powerful analysis. It produces accurate closed-loop shaker control and has high built-in safety mechanism that reduces the risks of damaged items.

The connections between each component are illustrated in Figure 4. The input excitation for moving the shaker is generated by the software and then memorized by SCADAS. The controller card will give the signal to the amplifier and then the amplifier will generate the vibration to the shaker. Three accelerometers are placed in this study to measure the acceleration taken from the base, first floor, and second floor of the building structure. Once the accelerometer detects the movement, the signal is sent to SCADAS DAC in acceleration value and recorded by the LMS Test.Lab software in the PC. The parameters for the experimental system parameter are shown in Table 1.

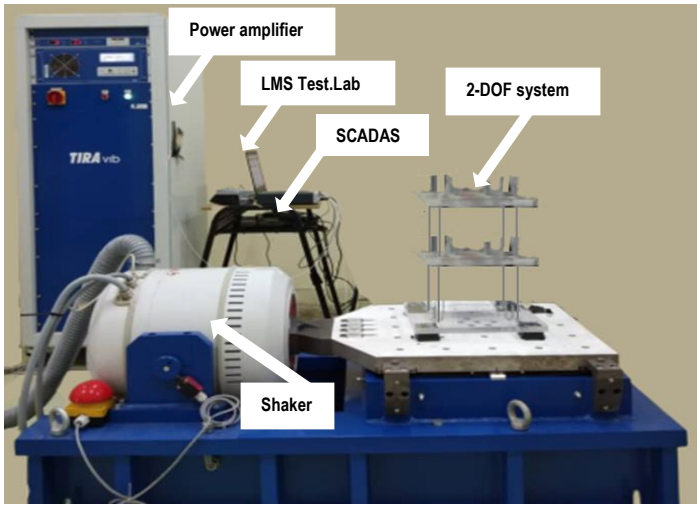

Figure 3 Experimental setup

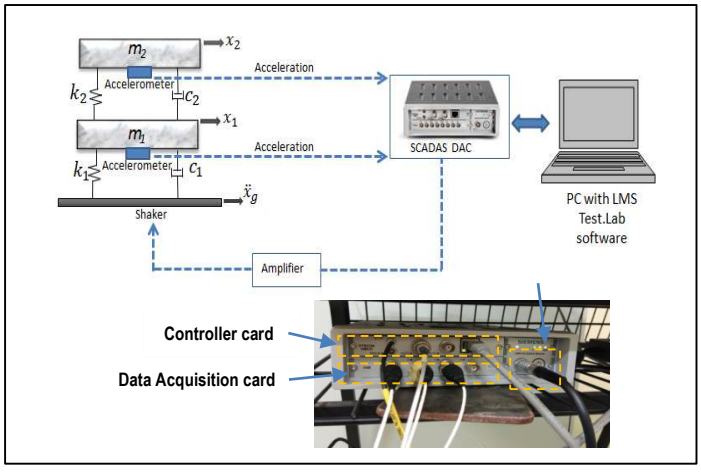

Figure 4 Experimental work connection

Table 1 Experimental system parameter

Parameter	Unit	Value
Mass (Floor 1 and 2)	kg	764.00
Stiffness (Floor 1 and 2)	N/m	182.9
Damping (Floor 1 and 2)	Ns/m	30
Accelerometer sensitivity	mV/G	10
Shaker frequency range	Hz	2-4000
Amplifier output power	VA	4200
Field voltage	V	100
Field current	A	6
Signal to noise ratio	db	> 80

Before running the experiment, it is required to pre-test the closed-loop system by configuring the SelfCheck setting. SelfCheck configuration is used to verify the experimental setup according to the connection, amplifier, and shaker problems. If problems occur, the status in the software window will appear "warning" or "not ok". In this case, the status showing 'Open Channel' appeared. This is because the connection between the accelerometer and data acquisition card output is not stable. The accelerometer channel did not generate a significant result above the background noise level. Other problems that occured were caused by DAC issues while running the SelfCheck configuration. The DAC issue occurs because of the situation by the shaker amplifier that has not enough output to run the full-scale equipment. The explanation of the overall process for the validation of the system is shown in Figure 5.

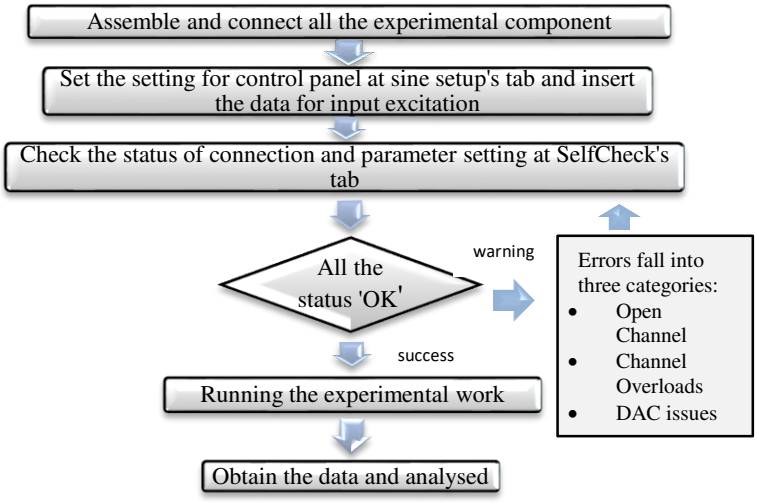

Figure 5 Flowchart of the experimental work

3. Control Strategies

Consider the building structure as;

$$\begin{cases} \dot{x}_1 = x_2 \\ \dot{x}_2 = f(x) + g(x)u \ + d(x) \end{cases} \tag{6}$$

where the system state vector, $x = [x_1, x_2, x_d]^T$, $f(x)$ and $g(x) \neq 0$ are nonlinear function of x, $d(x)$ is uncertainties and disturbance and u is the scalar control input.

3.1 Terminal sliding mode control

The terminal sliding surface is described as (7) where β is a design constant that must be more remarkable than 0, and the value of p and q are positive odd integers that meet the condition; $p > q$.

$$s = x_2 + \beta x_1^{q/p} \tag{7}$$

$$u = -g^{-1}(x)[f(x) + \beta \frac{q}{p} x_1^{\frac{q}{p}-1} x_2 + (l_g + \eta) sgn\,(s)] \tag{8}$$

where $\eta > 0$.

Stability analysis for TSMC is described as;

$$\dot{s} = \dot{x}_2 + \beta \frac{q}{p} x_1^{\frac{q}{p}-1} \dot{x}_1 \tag{9}$$

$$= f(x) + g(x)u + d(x) + \beta \frac{q}{p} x_1^{\frac{q}{p}-1} \dot{x}_1 \tag{10}$$

Substitute the equation (8) into (10) to obtain;

$$= d(x) - (l_g + \eta) sgn(s) \tag{11}$$

$$s\dot{s} = sd(x) - (l_g + \eta)|s| \leq -\eta|s| \tag{12}$$

Based on the equation state in (12), if the value for $x_2 \neq 0$ when $x_1 = 0$, the singularity occurs. This causes the problem to occur in the reaching phase when the state reaches at $s = 0$. This issue is solved by using nonsingular TSMC.

Finite-time analysis for the system is derived based on the following equation;

$$\int_{s=s(0)}^{s=s(t_r)} ds = \int_o^{tr} \pm n dt \tag{13}$$

$$s(t_r) - s(0) = \pm n t_r \tag{14}$$

$$t_r = \frac{s(0)}{n} \tag{15}$$

Suppose that after time t_r, the attaining time which is the time of switching trajectory reach at sliding surface, t_s from $x_1(t_r) \neq 0$ to $x_1(t_r + t_s) = 0$. In this phase $s = 0$,

$$x_2 + \beta x_1^{q/p} = 0 \tag{16}$$

$$\dot{x}_1 = -\beta x_1^{q/p} \tag{17}$$

Then, the equation in (17) is integrated to obtain equation (18) written as;

$$\int_{x_1(t_r)}^{0} x_1^{q/p} dx_1 = \int_{t_r}^{t_r+t_s} -\beta dt \tag{18}$$

$$-\frac{p}{p-q} x_1^{1-\frac{q}{p}}(t_r) = -\beta t_s \tag{19}$$

$$t_s = \frac{p}{\beta(p-q)} |x_1(t_r)|^{1-q/p} \tag{20}$$

3.2 Nonsingular terminal sliding mode control

Terminal sliding mode control type nonsingular has an advantage in giving a fast dynamic response, finite-time convergence, high control precision, and can eliminate the abnormal phenomena in the control input of the system.

$$s = x_1 + \frac{1}{\beta} x_2^{\frac{p}{q}} \tag{21}$$

$$u = -g^{-1}(x)[f(x) + \beta \frac{q}{p} x_2^{2-\frac{p}{q}} + \left(l_g + \eta\right) + sgn(s)] \tag{22}$$

Where $\beta > 0$, p and q are both positive odd numbers, $1<p/q<2$, η is greater than zero and l_g is estimated using adaptive law.

Analysis of stability for NTSMC is written as;

$$\dot{s} = \dot{x}_1 + \frac{1}{\beta}\frac{p}{q} x_2^{\frac{p}{q}-1} \dot{x}_2 \tag{23}$$

$$= x_2 + \frac{1}{\beta}\frac{p}{q} x_2^{\frac{p}{q}-1} (f(x) + g(x)u + d(x)) \tag{24}$$

Substitute equation (22) into (24) to obtain;

$$= \frac{1}{\beta}\frac{p}{q} x_2^{\frac{p}{q}-1} (d(x) - (l_g + \eta) \tag{25}$$

$$s\dot{s} = \frac{1}{\beta}\frac{p}{q} x_2^{\frac{p}{q}-1} (sd(x) - (l_g + \eta)|s|) \tag{26}$$

$$s\dot{s} \leq -\frac{1}{\beta}\frac{p}{q}\, \eta x_2^{\frac{p}{q}-1} |s| \tag{27}$$

When $x_2 \neq 0$, $x_2^{\frac{p}{q}-1} > 0$ as to p and q are positive integers. This result in the equation (28) and it can be concluded that the condition for Lyanpunov is satisfied in the case of $x_2 \neq 0$.

$$-\frac{1}{\beta}\frac{p}{q}\, \eta x_2^{\frac{p}{q}-1} > 0 \tag{28}$$

The condition when $x_2 = 0$ is studied by substituting equation (28) into (29) written as;

$$\dot{x}_2 = g(x) - \beta \frac{q}{p} x_2^{2-\frac{p}{q}} - \left(l_g + \eta\right) sgn(s) \tag{29}$$

$$\dot{x}_2 = g(x) - (l_g + \eta) sgn(s) \tag{30}$$

Since we have $s > 0$, $\dot{x}_2 \leq -\eta$ and when $s < 0$, $\dot{x}_2 \geq \eta$, therefore the switching line $s = 0$ can be reach in finite time. The sliding mode $s = 0$ can be obtained from anywhere with the condition of switching trajectories in finite time.

3.3 Adaptive nonsingular terminal sliding mode control

RBFNN provide a global approximation of training data gives advantages of a simple structure and excellent learning ability. This method has the capability to approximate the uncertainties of unknown bound with universal error. Therefore, this technique is used in this study to estimate the value of the upper bound of an uncertain parameter, l_g. The equation for l_g is written in (31), and the output hidden layer, $\emptyset_i(x)$ is written in (32). Where, ϑ_i is threshold hidden layer, m_i the central position for neuron, and σ_i is neuron width. The structure of RBFNN is shown in Figure 6, which consists of three layers. The number of input and output neuron in RBFNN are determine by the problem data. The first layer of RBFNN is the input layer determined by equating the number of input variables in the process data which are displacement and velocity data.

Five neurons in the hidden layer are the connective weight between hidden and output neurons, w_T (w_1,w_2,w_3,w_4,w_5) is determined using rule-of-thumb method. It is crucial to find the correct number of neurons in the hidden layer because too few neurons will result in underfitting. Underfitting occurs when a number of neurons in the hidden layer are difficult to detect the signals in a complicated data set. Meanwhile, too many neurons in the hidden layer can cause overfitting and this problem may occur when neural networks have so much information processing capacity. Therefore, the calculation on this hidden layer neuron, N_h is calculated in Equation (36). Where, N_T is the number of samples in training data set, $\propto$ is arbitrary scaling factor , N_i is number of input neuron and N_o is number of output neuron. The data of displacement and acceleration responses along 30s for El Centro and 320s for Southern Sumatra excitation from the building are trained to estimate the uncertain parameter in NTSMC. The output for RBFNN is depends on the values of the input, centroids, widths, weights and biases. During the training, all these values are computed to estimate the appropriate output value. After the training completed, the estimation of uncertainties unknown bound can be predicted.The output for the trained RBFNN is 0.845.

The steps on designing ANTSMC in this study are as follow;

1) Simplify the system into $\dot{x}_1$and $\dot{x}_2$
2) Design sliding variables
3) Design NTSMC with an unknown parameter for ANTSMC, RBFNN
4) Perform stability analysis by satisfied Lyapunov condition
5) Perform analysis on attaining time
6) Construct in Simulink and apply to the system

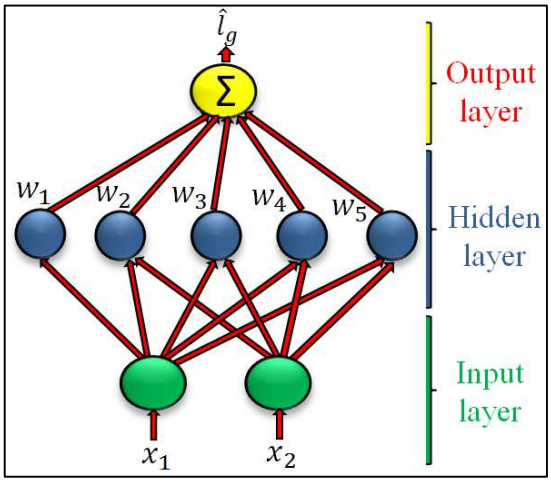

Figure 6 RBFNN structure

$$l_g = w^T \emptyset_i(x) + \vartheta_i \tag{31}$$

$$\emptyset_i(x) = \exp\left(-\frac{||x - m_i||^2}{\sigma_i^2}\right) \tag{32}$$

$$\hat{w} = |s| M \emptyset_i(x) \tag{33}$$

Where,

$$M = \frac{1}{\beta}\frac{p}{q} x_2^{\frac{p}{q}-1} \geq 0 \tag{34}$$

$$N_h = \frac{N_T}{[\propto\times (N_i + N_o)]} \tag{35}$$

3.4 Controls of Structure System

The measurement for the sliding variable is obtained by using the mathematical model described by equations (7) and (21). The values of p and q must be positive odd numbers. After applying all the assumption values, the best performance response is obtained when the values are set to 5 and 3. The terminal sliding variables, s and control design, u for each controller used are;

$$s_{TSMC} = x_2 + x_1^{3/5} \tag{36}$$

$$s_{NTSMC} = x_1 + x_2^{5/3} \tag{37}$$

$$s_{ANTSMC} = x_1 + x_2^{5/3} \tag{38}$$

Theorem 1.
After applying the control law in (40) into the building structure (1), suppose that the sliding variable in (37) and (38) will converge to zero in finite time, and the proposed controller can guarantee robustness and stability of the system. The controller design for the building structure is derived as;

$$u_{TSMC} = k_d x_1 + c_d \dot{x}_1 - M_T \beta \frac{q}{p} x_1^{\frac{q}{p}-1} \dot{x}_2 - M_T(\xi + \eta) sgn(s) \tag{39}$$

$$u_{NTSMC} = k_d x_2 + c_d \dot{x}_2 - M_T \beta \frac{q}{p} x_2^{2-\frac{p}{q}} - M(\xi + \eta) + sgn(s) \tag{40}$$

Proof 1.
The proof for Theorem 1 is obtained through stability analysis of this controller. Consider that the Lyapunov function candidate is V= ½ s^2. Then the derivative of V along the trajectory is

$$\dot{V} = s\dot{s} \tag{41}$$

$$\dot{s} = \dot{x}_1 + \frac{1}{\beta}\frac{p}{q} x_2^{\frac{p}{q}-1} \dot{x}_2 \tag{42}$$

$$\dot{s} = x_2 + \frac{1}{\beta}\frac{p}{q} x_2^{\frac{q}{p}-1} [-\frac{k_T}{M} x_1 - \frac{c_T}{M} + \frac{1}{M}(u - f_d)] \tag{43}$$

Substitute equation (40) into (43), resulting in equation (45) as shown below; (44)

$$\dot{s} = x_2 + \frac{1}{\beta}\frac{p}{q} x_2^{\frac{p}{q}-1} [-\frac{k_f}{M_T} x_1 - \frac{c_f}{M_T} + \frac{f_d}{M_T} + \frac{\left[k_f x_1 + c_f x_1 - M_T \beta \left(\frac{q}{p}\right) x_2^{2-\frac{p}{q}} - M_T(\xi+\eta) sgn(s)\right]}{M_T}] \tag{45}$$

$$\dot{s} = x_2 + \frac{1}{\beta}\frac{p}{q}x_2^{\frac{p}{q}-1}[-\frac{f_d}{M_T} - \beta\left(\frac{q}{p}\right)x_2^{2-\frac{p}{q}} - (\xi + \eta)sgn(s) \quad (46)$$

$$\dot{s} = -(\xi + n)sgn(s) - \frac{f_d}{M} \quad (47)$$

The sliding surface estimation error is written as;

$$s_e = s - \hat{s} = \hat{x}_2 \quad (48)$$

This yields equation (49), where ξ is the adaptive law value.

$$\dot{V} = s\dot{s} = (s - \hat{s} + \hat{s})(-\frac{f_d}{M} - (\xi + \eta)sgn(\hat{s})) \quad (49)$$

$$\dot{V} = (s - \hat{x}_2)(-\tfrac{f_d}{M} - (\xi + \eta)sgn(\hat{s})) \quad (50)$$

Solve the equation above and obtain the equation as follows;

$$\dot{V} = -\tfrac{f_d}{M}s + \tfrac{f_d}{M}\hat{x}_2 - (\xi + \eta)sgn|\hat{s}| + \hat{x}_2(\xi + \eta)sgn(\hat{s}) \quad (51)$$

Where $\frac{f_d}{M} \leq \xi$,

$$\dot{V} = \hat{s}\xi + \hat{x}_2 - (\xi + \eta)sgn|\hat{s}| + \hat{x}_2(\xi + \eta) \quad (52)$$

$$\dot{V}(t) = \dot{s}s =\leq -\eta|\hat{s}| \quad (53)$$

That is,

$$\dot{V} \leq -\eta|s| < 0 \text{ for } s \neq 0 \quad (54)$$

According to equation (54), the Lyapunov controller stability of ANTSMC for the building structure can be evaluated. In this study the value of η is 0.01, and the sliding surface is taken with the value of $|2\times10^5|$ resulted -0.02×10^5. Therefore, the value obtained is below than 0, thus, proving that the stability of the controller, NTSMC manifold converges to zero in finite time. On the other hand, if (38) is reached, the output tracking error of the building structure will converge to zero in finite time and prove the robustness and the stability of the system. This completes the proof for Theorem 1.

This study uses two inputs, one output, and five hidden neurons. The block diagram consists of an adaptive NTSM with the building structure is shown in Figure 7, where x_f is the desired value for the system output, e is error, s is sliding mode, u is the control input, and the output feedback is displacement and velocity of the building structure.

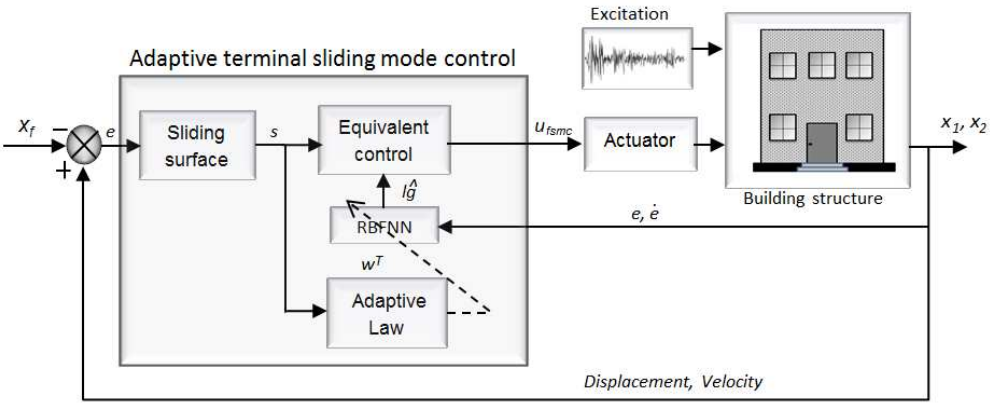

Figure 7 Block diagram of the system with the adaptive NTSMC

4. Result and Discussion

4.1 System validation

The building structure model constructed in Matlab are validated via an experimental setup measured by the LMS.Test lab software. Since accelerometers are used in this experimental work, the input and output of the miniature building used are measured in acceleration value. Various input are given to validate the buidling structure model. The acceleration results were measured using the accelerometer as shown in Figure 8 (a), (b) and (c) for ground input, second floor and first floor with the range of 0.78 m/s^2, 0.01 m/s^2, and 0.1 m/s^2, respectively.

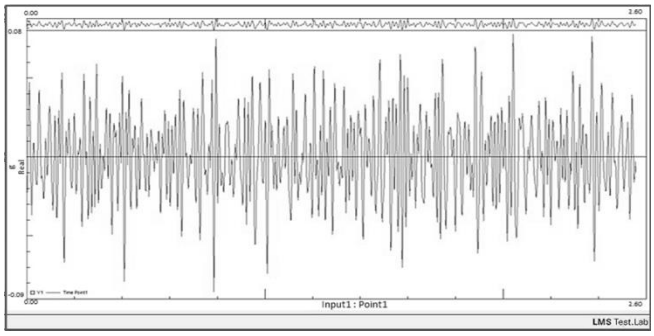

(a)

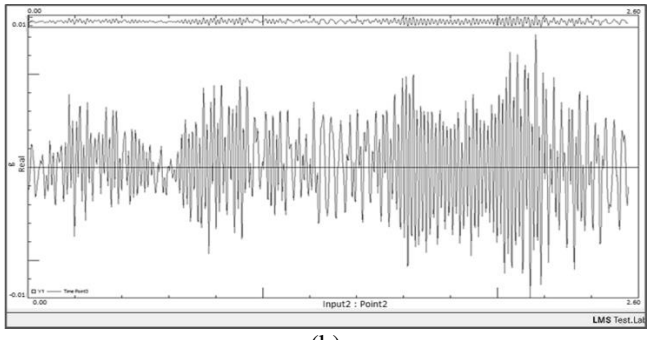

(b)

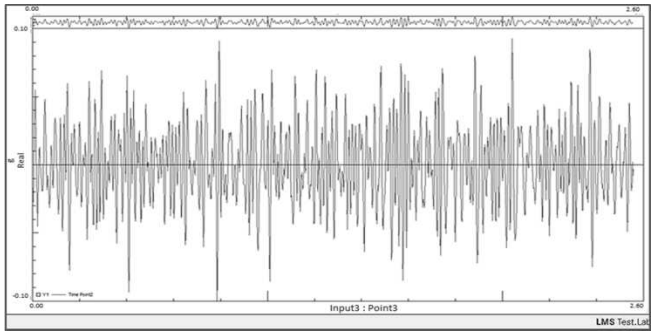

(c)

Figure 8 Acceleration responses measured from the experimental work (a) ground input (b) first floor (c) second floor

The results of the experimental work and simulation are compiled in Figure 9. As can be seen from these figures, the results of both methods have the same minimum and maximum values. The acceleration ranges for the first and second storeys are ± 0.01 m/s^2 and ± 0.1 m/s^2, respectively.

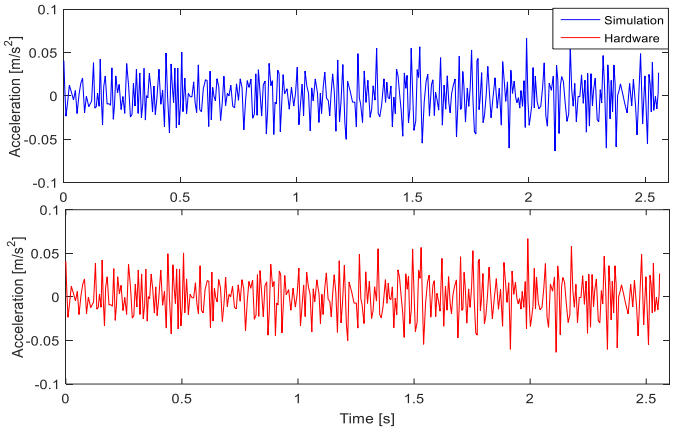

(a)

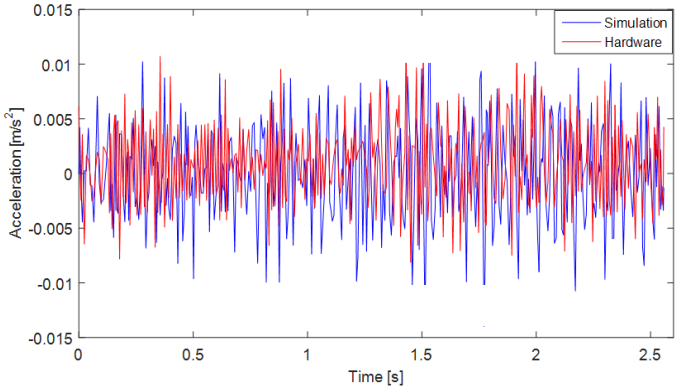

(b)

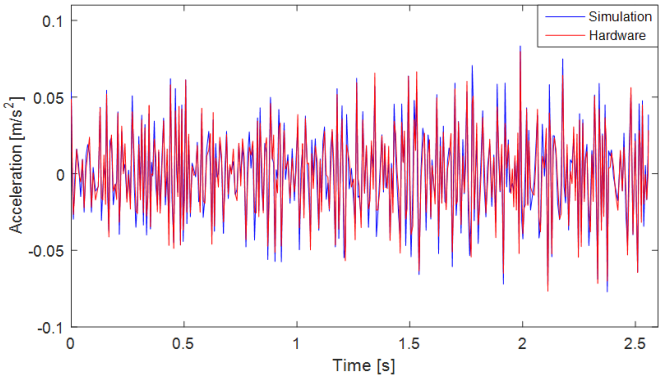

(c)

Figure 9 Comparison of the simulation and experimental results (a) ground input (b) second floor (c) first floor

4.2 Implementation of the control strategy

The building structure is equipped with HMD together with the implementation of the control strategy. The actual parameter for the building structure is used to evaluate the effectiveness of the controller in real life as shown in Table 2. Two input excitations are given as disturbances to study the robustness of the control strategy towards the system taken from the real earthquake occurred in El Centro in 1960 with the magnitude of 6.9 M_w and Southern Sumatra on 12 September 2007 with the magnitude of 8.4 M_w.

Table 2 System parameter

Number of floors	Mass ($10e^3$kg)	Stiffness ($10e^5$N/m)	Damping ($10e^5$N.s/m)
First and second	320	930	15.69
HMD	44	36.7	0.71

The results obtained for the building structure with both excitations are shown in Figure 10 for the second and first floors, respectively. The result shows that the implementation of control strategies has successfully suppressed the earthquake-induced vibrations. The maximum vibration occurred at 2.17 s causing the reduction percentage measured at the second floor with respect to the uncontrolled system generated by each controller to be 46% for ANTSMC, 36% for NTSMC, and 10% for TSMC. The reduction percentage generated by the first floor is 40% for ANTSMC, 38% for NTSMC, and 7.5% for TSMC. This shows that the ANTSMC has the highest reduction percentage compared to the other controllers.

The second excitation taken from Southern Sumatra with the duration of acceleration is longer compared to the El Centro earthquake which is 320.725 s. The results obtained are shown in Figure 11 for both floors of the building. The maximum vibration recorded for the second and first floors are 1.3×10^{-3} m and 0.78×10^{-3} m, respectively. Based on these maximum displacement values, the percentage of vibration reduction from the uncontrolled structure for each control strategy is 42% by NTSMC, 38% by NTSMC, and 19% by TSMC. After the implementation of control strategies, it was shown that ANTSMC has the superior performance in suppressing the building vibration.

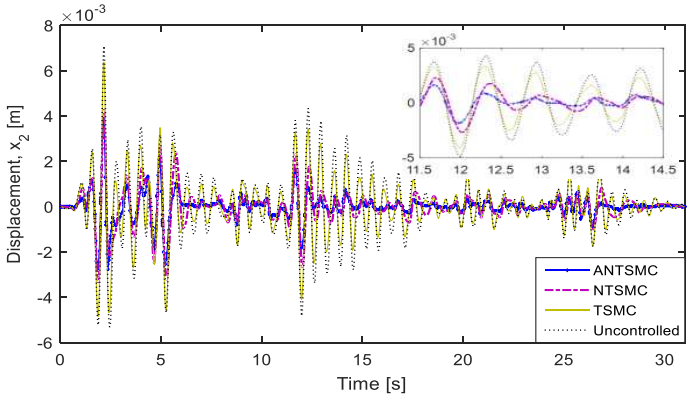

(a)

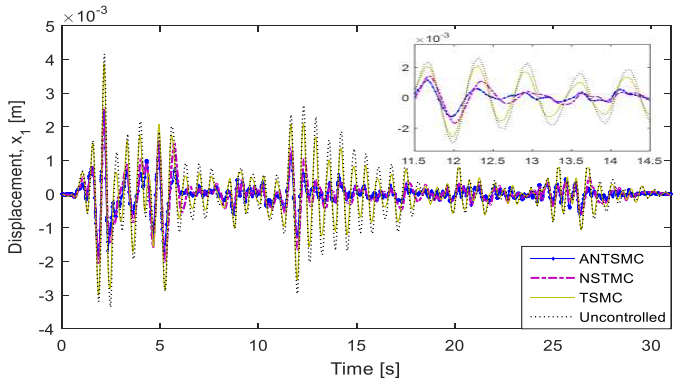

(b)

Figure 10 Comparison of the displacement responses for the building structure at the (a) second floor (b) first floor for the El Centro excitation

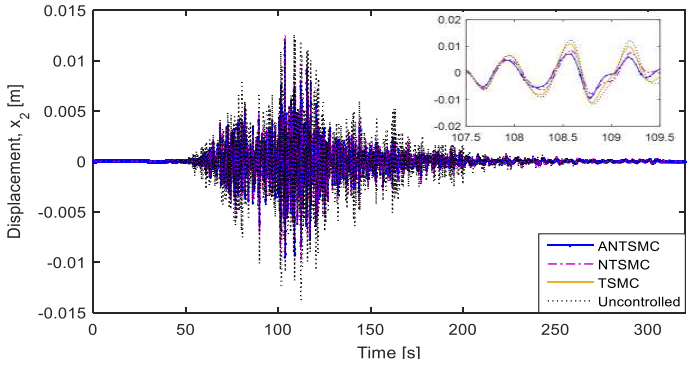

(a)

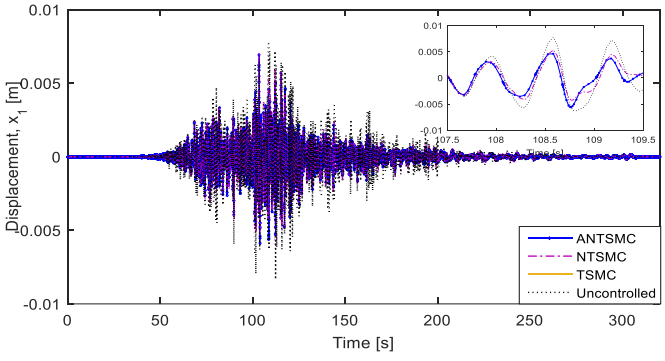

(b)

Figure 11 Comparison of the displacement responses for the building structure at the (a) second floor (b) first floor for the Southern Sumatra excitation

The sliding surface measured by the El Centro excitation for each controller is shown in Figure 12. The sliding surface design should reflect the required specification when the sliding mode is established. The figures show that the state trajectories are moving towards the sliding surface that was set to 0 to maintain the position of the system during an earthquake. This has fulfilled the system with a required response to obtain a stable condition. The same time was setting for each controller and resulting the state trajectory generated by the ANTSMC has a faster response to reach the desired sliding surface compared to NTSMC and TSMC.

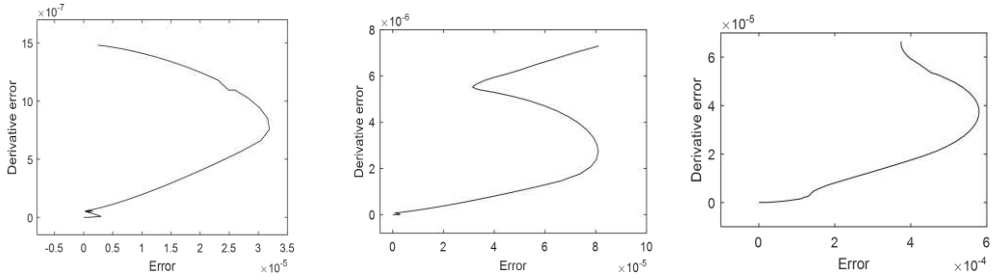

(a) (b) (c)

Figure 12 Sliding surface for (a) ANTSMC (b) NTSMC (c) TSMC

The results are summarized in Figure 13 for both excitations measured at the first and second floor taken at the maximum vibration of the building structure which occurred at 2.17 s for the El Centro and 108.6 s for the Southern Sumatra excitations. According to both figures, the second floor generated a higher sway during the seismic activity than the first floor. However, when control strategies were applied, the vibrations were suppressed.

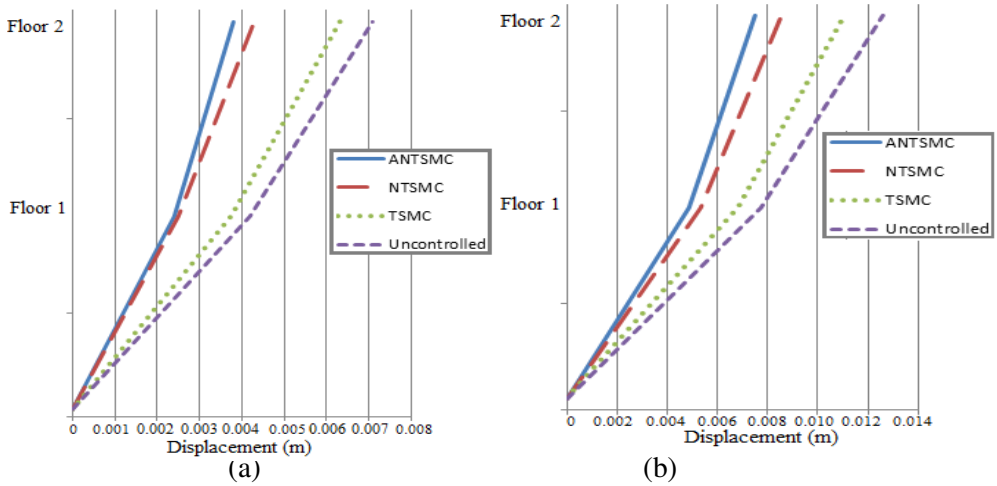

(a) (b)

Figure 13 The building response with the control strategy at each floor with the input excitations of (a) El Centro (b) Southern Sumatra

This study considers the ductile reinforced concrete building and the building collapse probability is measured according to the graph damage of probability for the low-rise building under the 3-DOF system according to the guildeline given by FEMA (2003) and structural performance under seismic load by Incremental Dynamic Analysis (IDA) (Vamvatsikos and Cornell 2002). Based on the probability of the building collapse for both excitations, it is clear that the implementation of the proposed controller which is the ANTSMC in the 2-DOF structure has reduced the percentage of the building from collapse. From Figure 14 (a), the percentage of the building to have slight damage is 98%, and after the implementation of the ANTSMC, the probability is reduced to 50%. Moreover, the probability percentage of the building to have moderate damage is reduced tfrom 76% to 26%, extensive damage is reduced from 25% to 6% and complete damage is reduced from 0.8% to 0.2%, respectively. From Figure 14 (b), the probability of the building to have slight damage is 100% which is reduced to 98% after implementation of ANTSMC. For moderate damage, the damage probability has reduced from 95% to 75%, extensive damage from 40% to 22% and complete damage is reduced from 15% to 0.8%, respectively. This controller shows a high percentage reduction when applied to the system that is triggered by the El Centro earthquake rather than by the Southern Sumatra earthquake since the magnitude of the El Centro earthquake is lower than the magnitude of the Southern Sumatra earthquake. However, both responses show impressive results in reducing the probability of the building collapse when implemented with the controller.

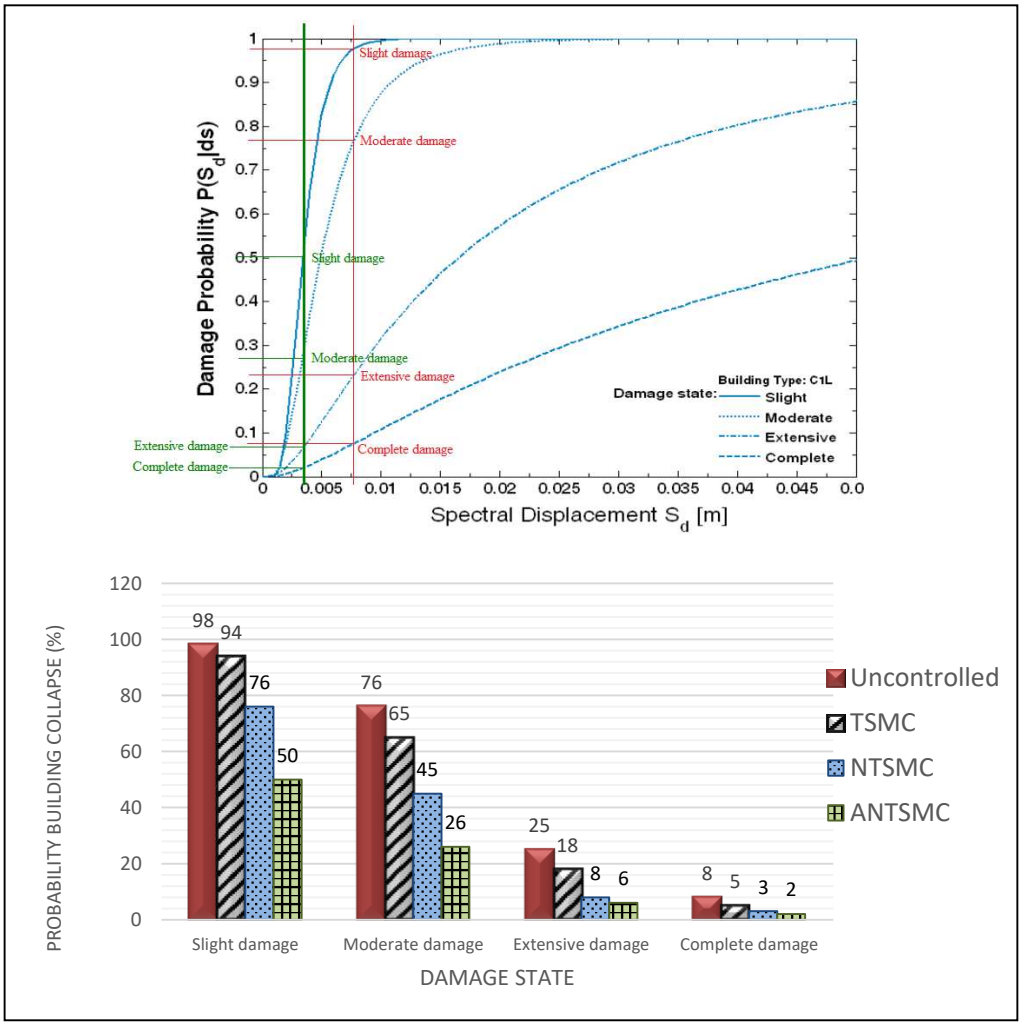
Damage Probability P(S_d|ds)
Spectral Displacement S_d [m]
Slight damage
Moderate damage
Slight damage
Moderate damage
Extensive damage
Complete damage
Extensive damage
Complete damage
Building Type: C1L
Damage state:
Slight
Moderate
Extensive
Complete
PROBABILITY BUILDING COLLAPSE (%)
98
94
76
50
76
65
45
26
25
18
8
6
8
5
3
2
Slight damage
Moderate damage
Extensive damage
Complete damage
DAMAGE STATE
Uncontrolled
TSMC
NTSMC
ANTSMC

(a)

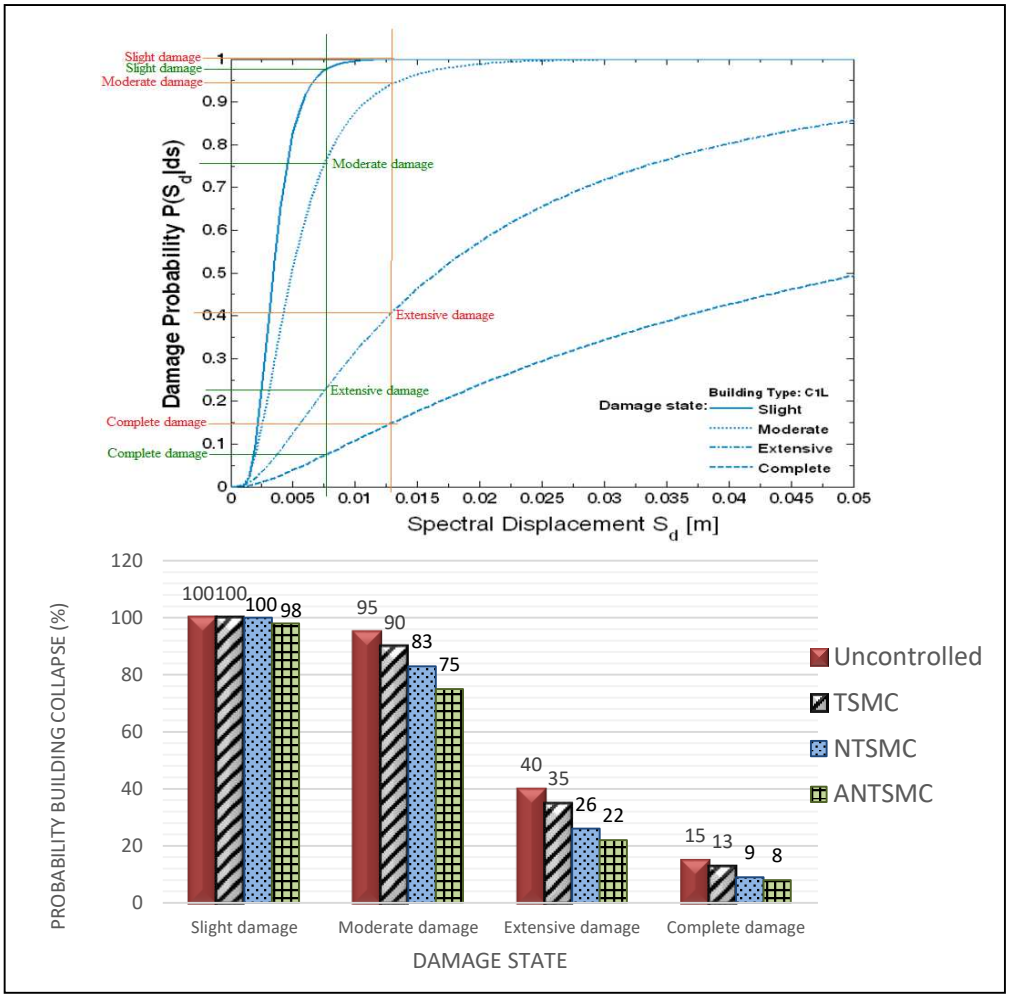

(b)

Figure 14 Probability of collapse for the building structure with ANTSMC with the input excitations of (a) El-Centro (b) Southern Sumatra

5. Conclusion

This study was aimed at investigating the influence of implementing the control strategy, namely ANTSMC to the 2-DOF structure in enhancing the building's structural and decreasing the risk of the building from damage. The system was validated by the experimental work for the 2-DOF structure and acceleration responses were measured by the LMS Test.Lab software. The result for the building system response was compared to the simulation result in Simulink. ANTSMC was designed to enhance the performance of the building structure by suppressing the vibration during an earthquake. The effectiveness of the controller was compared with TSMC and NTSMC. The stability of ANTSMC was demonstrated as the building structure reached its equilibrium faster and maintained its position as the desired response stated. Moreover, the proposed control strategy reduced the probability of damage to the building structure. The probability percentage of the building to have slight damage with the implementation of ANTSMC was reduced until 50% compared to an uncontrolled building with a probability of 98% to have a slight damage. The lower percentage in having the probability of the building experiencing damage shows the significant impact of the implementation of control strategy in the building structure.

Acknowledgement

The authors would like to acknowledge Universiti Teknologi Malaysia (research grant Professional Development Research University: Q.K130000.21A2.05E38) for financially supporting this research.

Conflict of interest

All authors declare that they have no conflicts of interest.

References

Abu-Faraj ZO, Hamdan TF, Wehbi MR, et al (2008) The study of postural stability in an earthquake-simulated environment yields a retained cognitive learning outcome. J Biomed Pharm Eng 2:14–21

Alam J, Hussan M, Sarraz A (2017) Seismic Fragility Assessment of RC Building using Nonlinear Static Pushover Analysis. 26:7

Allen RM, Melgar D (2019) Earthquake early warning: Advances, scientific challenges, and societal needs. Annu Rev Earth Planet Sci 47:361–388

Ansal A, Kurtuluş A, Tönük G (2010) Seismic microzonation and earthquake damage scenarios for urban areas. Soil Dyn Earthq Eng 30:1319–1328 https://doi.org/10.1016/j.soildyn.2010.06.004

Ba DX, Yeom H, Bae J (2019) A direct robust nonsingular terminal sliding mode controller based on an adaptive time-delay estimator for servomotor rigid robots. Mechatronics 59:82–94. https://doi.org/10.1016/j.mechatronics.2019.03.007

Bayrak OF, Bikçe M, Erdem MM (2021) Failures of structures during the January 24, 2020, Sivrice (Elazığ) Earthquake in Turkey. Nat Hazards 1–27 https://doi.org/10.1007/s11069-021-04764-z

Bhaiya V, Bharti SD, Shrimali MK, Datta TK (2019) Performance of semi-actively controlled building frame using mr damper for near-field earthquakes. In: Recent Advances in Structural Engineering, Volume 2. Springer, pp 397–407

Cao L, Chen X, Sheng T (2013) Fault tolerant small satellite attitude control using adaptive non-singular terminal sliding mode

Chesné S, Collette C (2018) Experimental validation of fail-safe hybrid mass damper. J Vib Control 24:4395–4406

Chesné S, Inquieté G, Cranga P, et al (2019) Innovative Hybrid Mass Damper for Dual-Loop Controller. Mech Syst Signal Process 115:514–523. https://doi.org/10.1016/j.ymssp.2018.06.023

Cremen G, Velazquez O, Orihuela B, Galasso C (2021) Predicting approximate seismic responses in multistory buildings from real-time earthquake source information, for earthquake early warning applications. Bull Earthq Eng 1–21 https://doi.org/10.1007/s10518-021-01088-y

D'Ayala D, Ansal A (2012) Non linear push over assessment of heritage buildings in Istanbul to define seismic risk. Bull Earthq Eng 10:285–306 https://doi.org/10.1007/s10518-011-9311-1

Djedoui N, Ounis A, Pinelli JP, Abdeddaim M (2017) Hybrid Control Systems For Rigid Buildings Structures Under Strong Earthquakes. ASIAN J Civ Eng 18:893–909

Duan X, Pappin JW (2008) A Procedure For Establishing Fragility Functions For Seismic Loss Estimate Of Existing Buildings Based On Nonlinear Pushover Analysis. 14th World Conf Earthq Eng

Federal Emergency Management Agency (FEMA) (2003) HAZUS-MH MR4 Multi-Hazar d Loss Estimation Methodology – Earthquake Model: Technical Manual. Department of Homeland Security

Giordano N, De Luca F, Sextos A, et al (2021) Empirical seismic fragility models for Nepalese school buildings. Nat Hazards 105:339–362 https://doi.org/10.1007/s11069-020-04312-1

Gkimprixis A, Tubaldi E, Douglas J (2020) Evaluating alternative approaches for the seismic design of structures. Bull Earthq Eng 18:4331–4361 https://doi.org/10.1007/s10518-020-00858-4

Grünthal G, Musson RMW (2020) Earthquakes, intensity. Encycl Solid Earth Geophys 1–7

Gupta HK, Sabnis KA, Duarah R, et al (2020) Himalayan Earthquakes and Developing an Earthquake Resilient Society. J Geol Soc India 96:433–446 https://doi.org/10.1007/s12594-020-1581-2

Liu J (2013) Radial Basis Function (RBF) Neural Network Control for Mechanical Systems https://doi.org/10.1007/978-3-642-34816-7

Liu J, Wang X (2012) Advanced Sliding Mode Control for Mechanical Systems: Design, Analysis and MATLAB Simulation. Springer Science & Business Media https://doi: 10.1007/978-3-642-20907-9

Mamat N, Yakub F, Shaikh Salim SAZ, Mat Ali MS (2020) Seismic vibration suppression of a building with an adaptive nonsingular terminal sliding mode control. J Vib Control 26:2136–2147 https://doi.org/10.1177/1077546320915324

Martins L, Silva V (2020) Development of a fragility and vulnerability model for global seismic risk analyses. Bull Earthq Eng 1–27 https://doi.org/10.1007/s10518-020-00885-1

Mitchell R, Kim Y, El-Korchi T, Cha YJ (2013) Wavelet-neuro-fuzzy control of hybrid building-active tuned mass damper system under seismic excitations. JVC/Journal Vib Control 19:1881–1894. https://doi.org/10.1177/1077546312450730

Ning D, Sun S, Du H, et al (2018) Control of a multiple-DOF vehicle seat suspension with roll and vertical vibration. J

687 Sound Vib 435:170–191. https://doi.org/10.1016/j.jsv.2018.08.005
688 Peyghaleh E, Mahmoudabadi V, Martin JR, et al (2018) Impact of local site conditions on portfolio earthquake loss
689 estimation for different building types. Nat Hazards 94:121–150 https://doi.org/10.1007/s11069-018-3377-x
690 Robinson TR, Rosser NJ, Densmore AL, et al (2018) Use of scenario ensembles for deriving seismic risk. Proc Natl Acad
691 Sci 115:E9532–E9541. https://doi.org/10.1073/pnas.1807433115
692 Thenozhi S, Yu W (2013) Advances in modeling and vibration control of building structures. Annu Rev Control 37:346–
693 364 https://doi.org/10.1016/j.arcontrol.2013.09.012
694 Vamvatsikos D, Cornell CA (2002) Incremental dynamic analysis. Earthq Eng Struct Dyn 31:491–514
695 https://doi.org/10.1002/eqe.141
696 Xing H, Junyi S, Jin H (2020) The casualty prediction of earthquake disaster based on Extreme Learning Machine method.
697 Nat Hazards 102:873–886 https://doi.org/10.1007/s11069-020-03937-6
698 Xu B (2014) Integrated optimization of structure and control systems for interconnected building structures subjected to
699 earthquake. J Vib Control 20:1318–1332
700 Xu W, Jiang Y, Mu C, Yue H (2015) Nonsingular terminal sliding mode control for the speed regulation of permanent
701 magnet synchronous motor with parameter uncertainties doi: 10.1109/IECON.2015.7392393.
702 Vazurkar UY, Chaudhari DJ (2016) Development of Fragility Curves for RC Buildings. Int J Eng Res 5:591–594.
703 https://doi.org/10.17950/ijer/v5i3/016
704 Zamani A-A, Tavakoli S, Etedali S, Sadeghi J (2018) Online tuning of fractional order fuzzy PID controller in smart
705 seismic isolated structures. Bull Earthq Eng 16:3153–3170
706 Zhu Z, Yan Y (2014) Space-based line-of-sight tracking control of GEO target using nonsingular terminal sliding mode.
707 Adv Sp Res 54:1064–1076. https://doi.org/10.1016/j.asr.2014.05.013
708 Zizouni K, Fali L, Sadek Y, Bousserhane IK (2019) Neural network control for earthquake structural vibration reduction
709 using MRD. Front Struct Civ Eng 13:1171–1182. https://doi.org/10.1007/s11709-019-0544-4
710